Quantum Semiclass. Opt. **9** (1997) 737–747. Printed in the UK PII: S1355-5111(97)81848-9

Effects of transverse-mode competition on the injection dynamics of vertical-cavity surface-emitting lasers

Joanne Y Law†, Guido H M van Tartwijk and Govind P Agrawal
The Institute of Optics, University of Rochester, Rochester, NY 14627, USA

Received 20 March 1997

Abstract. We investigate theoretically the static and dynamic characteristics of an optically injected vertical-cavity surface-emitting laser (VCSEL), under both single- and two-mode operation. Our model includes the spatial dependence of both the carrier density and the optical field. We find that within the locking range, a two-mode VCSEL can be forced to operate in a single transverse mode under appropriate conditions. Outside the locking range, the VCSEL shows a rich variety of nonlinear dynamics. Results show that the static and dynamic behaviours depend strongly on the frequency detuning, the injection power and the strength of the intermodal coupling induced by spatial hole burning. In particular, strong intermodal coupling can reduce the sensitivity of the VCSEL toward external injection, in terms of both static (locking) and dynamic (nonlocking) behaviours.

1. Introduction

Injection locking of lasers has been a subject of interest for many years. In particular, injection locking of semiconductor lasers remains an important research topic because of its potential for producing compact coherent sources. It is well known that the frequency of a semiconductor laser can be locked to that of the injected signal depending on the power and the frequency detuning of the injected signal [1]. Outside this locking regime, several interesting nonlinear phenomena such as four-wave mixing [2], the period-doubling route to chaos [3] and polarization bistability [4] have been studied.

Recently, a new class of semiconductor lasers, known as vertical-cavity surface-emitting lasers (VCSELs), has been developed. The unique geometry of VCSELs results in several significant advantages over their edge-emitting counterparts, including a low threshold current, single-longitudinal-mode operation, circular output-beam profile and wafer-scale integrability [5, 6]. These advantages make VCSELs quite promising as compact light sources for future applications in optical communications and interconnects. Experimental studies of injection locking show a dependence on the frequency detuning and the power of the injected signal that is similar to the case of edge-emitting semiconductor lasers [7]. Outside the locking region, VCSELs also exhibit rich nonlinear dynamics, such as four-wave mixing under single-mode operation [7] and polarization bistability under two-mode operation [8]. However, the theoretical modelling of VCSELs operating under injection conditions has neglected spatial effects so far [7]. Since VCSELs have relatively large transverse dimensions, effects such as spatial hole burning and carrier diffusion are expected to be important, especially because VCSELs often operate in several transverse modes at

† E-mail address: jlaw@optics.rochester.edu

1355-5111/97/050737+11$19.50 © 1997 IOP Publishing Ltd

high injection currents [9–11]. Such spatial effects are expected to affect the VCSEL operation under optical injection considerably.

In this paper, we investigate theoretically the injection dynamics of VCSELs under both single- and two-mode operation. Our model, described in section 2, includes the spatial dependence of both the optical field and the carrier density. Section 3 presents the locking regions obtained from an analytical solution of the single-mode spatially independent rate equations. Section 4 discusses the effects of spatial hole burning and two-mode operation on the locking regimes by comparing the numerical results with the analytical results obtained in section 3, and investigates the possibility of complete suppression of a higher-order transverse mode by injecting the external field into the fundamental mode only. The remainder of section 4 presents the injection dynamics outside the locking range and discusses the change in dynamics associated with two-mode operation due to spatial hole-burning effects.

2. Model

In this section, we present the complete model which includes the spatial variations of both the optical field and the carrier density. Assuming that the VCSEL can operate in two orthogonally polarized transverse modes simultaneously, the rate equations in the cylindrical coordinates can be written as [9]

$$\frac{\mathrm{d}E_1}{\mathrm{d}t} = \tfrac{1}{2}(1 - \mathrm{i}\alpha)[G_1(t) - \gamma_1]E_1 + \kappa\sqrt{P_{\mathrm{inj}}}\exp(-\mathrm{i}\,\Delta\omega\, t) \tag{1}$$

$$\frac{\mathrm{d}E_2}{\mathrm{d}t} = \tfrac{1}{2}(1 - \mathrm{i}\alpha)[G_2(t) - \gamma_2]E_2 \tag{2}$$

$$\frac{\partial N}{\partial t} = D\nabla_{\mathrm{T}}^2 N + \frac{J(r,\phi)}{qd} - \frac{N}{\tau_{\mathrm{e}}} - BN^2 - \frac{1}{d}\sum_{i=1}^{2} G_{\mathrm{local}}|E_i(t)|^2|\psi_i(r,\phi)|^2 \tag{3}$$

where $E_i(t)$ is the complex field amplitude of the ith transverse mode with the spatial distribution $\psi_i(r,\phi)$, $N(r,\phi,t)$ is the carrier density, α is the linewidth enhancement factor, and $G_i(t)$ and γ_i are the gain and cavity loss, respectively, for the ith mode. In equation (3), τ_{e} is the carrier lifetime due to nonradiative recombination, D is the diffusion coefficient, B is the spontaneous recombination coefficient, d is the thickness of the active layer and $J(r,\phi)$ is the injection current density. The local gain $G_{\mathrm{local}} = a_0 v_{\mathrm{g}}(N - N_{\mathrm{T}})$ is assumed to be linearly proportional to the local carrier density $N(r,\phi,t)$, where N_{T} is the carrier density at transparency, a_0 is the gain cross section and v_{g} is the group velocity. The modal gains $G_i(t)$ in equations (1) and (2) are obtained by calculating the spatial overlap between the local-gain profile and the spatial-intensity distribution $|\psi_i(r,\phi)|^2$ of that mode, given by [9]

$$G_i(t) = \frac{\langle G_{\mathrm{local}}(r,\phi,t)|\psi_i(r,\phi)|^2\cos^2(\beta_i z)\rangle}{\langle|\psi_i(r,\phi)|^2\cos^2(\beta_i z)\rangle} \tag{4}$$

where the angled brackets denote an average over the active volume and β_i is the propagation constant of the ith mode.

The last term on the right-hand side of equation (1) accounts for optical injection [1]. P_{inj} is the injected power in units of photon number and $\Delta\omega = \omega_{\mathrm{inj}} - \omega_0$ is the frequency detuning of the injected signal from the frequency ω_0 of the VCSEL mode under free-running conditions. κ is the injection parameter, given by [12]

$$\kappa = \frac{1}{\tau_{\mathrm{L}}}\left(\frac{1}{r_2} - r_2\right)\sqrt{\eta_{\mathrm{inj}}} \tag{5}$$

where $r_2 = \sqrt{R_2}$ is the output-mirror reflectivity, τ_L is the VCSEL round-trip time and η_{inj} is the coupling efficiency of the injected light to the optical field in the laser cavity. Since no analytical solutions can be found for equations (1)–(3), we first briefly discuss the analytical theory of injection locking developed for a single-mode semiconductor laser using spatially independent rate equations to gain a basic understanding of VCSEL operation under injection conditions [12].

In this study, we assume that the two transverse modes are orthogonally polarized. This is often the case in practice [6], because of effects such as stress [13], anisotropic optical properties [14], quantum-well strain, wafer nonuniformity or a misoriented substrate [15]. In some studies, coupling to two distinct carrier populations has been considered [16]. These two carrier populations are responsible for the two modes, each with a different polarization. In VCSELs with unstrained quantum wells, such a distinction is difficult to make, and we assume that the two modes experience gain from the same carrier population.

3. Spatially independent single-mode model

In this section, we neglect carrier diffusion ($D = 0$) and assume single-mode operation ($E_2 = 0$). Further, we linearize the gain $G_1(t)$ around the free-running laser threshold, $G_1(t) = \gamma_1 + a_0 v_g(N - N_{th})$ and assume a constant, carrier-independent lifetime $T_1 = \tau_e(1 + B\tau_e N_{th})^{-1}$. Using $\Delta N = N - N_{th}$ and $g = a_0 v_g$, equations (1)–(3) then reduce to

$$\frac{dE_1}{dt} = \tfrac{1}{2}(1 - i\alpha)g\Delta N(t)E_1(t) + \kappa\sqrt{P_{inj}}\exp(-i\Delta\omega t) \tag{6}$$

$$\frac{d\Delta N}{dt} = \gamma_1 P_0 - \frac{\Delta N(t)}{T_1} - [\gamma_1 + g\Delta N(t)]|E(t)|^2 \tag{7}$$

where P_0 is the photon density in the free-running laser

$$P_0 = \frac{J - J_{th}}{\gamma_1 q d}. \tag{8}$$

The locked solutions are obtained by setting the time derivatives to zero in equations (6) and (7). By writing $E_1(t)$ as

$$E_1(t) = \sqrt{P_L}\exp(-i\Delta\omega t - i\varphi_L) \tag{9}$$

the locked photon density P_L, the locked phase φ_L and the corresponding excess carrier density ΔN_L are given by

$$\kappa^2 P_{inj}(\gamma_1 + g\Delta N_L) = \left[\Delta\omega^2 - \alpha\Delta\omega g\Delta N_L + \tfrac{1}{4}(1 + \alpha^2)g^2\Delta N_L^2\right](\gamma_1 P_0 - \Delta N_L/T_1) \tag{10}$$

$$P_L = \frac{\gamma_1 P_0 - \Delta N_L/T_1}{\gamma_1 + g\Delta N_L} \tag{11}$$

$$\sin(\varphi_L + \tan^{-1}\alpha) = -\frac{\Delta\omega}{\kappa\sqrt{1 + \alpha^2}}\sqrt{\frac{P_L}{P_{inj}}}. \tag{12}$$

Note that, in principle, equation (10) allows for three solutions for each injection condition. Which of these three solutions, if any, are stable is determined by performing a stability analysis. Before doing that it is useful to note that equation (12) provides a necessary condition for locking:

$$|\Delta\omega| \leqslant \kappa\sqrt{1 + \alpha^2}\sqrt{\frac{P_L}{P_{inj}}}. \tag{13}$$

This is also known as the locking range as it indicates the region in $(P_{\mathrm{inj}}, \Delta\omega)$-space where injection locking is possible.

A linear stability analysis of the locked solution (equations (10)–(12)) shows that small perturbations from the steady state change with time as $\exp(zt)$, where z is a solution of a third-order polynomial:

$$D(z) = z^3 + d_2 z^2 + d_1 z + d_0 \tag{14}$$

with the coefficients

$$d_2 = \frac{1}{T_1} + g(P_{\mathrm{L}} - \Delta N_{\mathrm{L}}) \tag{15}$$

$$d_1 = gP_{\mathrm{L}}(\gamma_1 + g\Delta N_{\mathrm{L}}) + \tfrac{1}{4}(1+\alpha^2)g^2\Delta N_{\mathrm{L}}^2 + \Delta\omega(\Delta\omega - \alpha g\Delta N_{\mathrm{L}}) - \left(\frac{1}{T_1} + gP_{\mathrm{L}}\right)g\Delta N_{\mathrm{L}} \tag{16}$$

$$d_0 = gP_{\mathrm{L}}(\gamma_1 + g\Delta N_{\mathrm{L}})\left[\alpha\Delta\omega - \tfrac{1}{2}(1+\alpha^2)g\Delta N_{\mathrm{L}}\right] + \left(\frac{1}{T_1} + gP_{\mathrm{L}}\right)\left[\tfrac{1}{4}(1+\alpha^2)g^2\Delta N_{\mathrm{L}}^2 + \Delta\omega(\Delta\omega - \alpha g\Delta N_{\mathrm{L}})\right]. \tag{17}$$

After applying the Routh–Hurwitz criterion, we find that in order for a locked solution to be stable, the following three conditions have to be fulfilled simultaneously [17]:

$$d_2 > 0 \qquad d_2 d_1 > d_0 \qquad d_0 > 0. \tag{18}$$

It turns out that among the three possible locked solutions given by equations (10)–(12) at most one is stable. One of the solutions represents the 'anti-laser' state with a photon density close to zero and is clearly unstable. The two other solutions have similar photon densities, but differ in phase φ_{L}. One of them is a saddle point and should be ignored. The remaining solution may or may not exhibit a Hopf instability, which is accompanied by undamped relaxation oscillations. In figure 1, we summarize in the parameter space $(P_{\mathrm{inj}}, \Delta\omega)$ the various dynamical regions for typical VCSEL parameters. The two outer

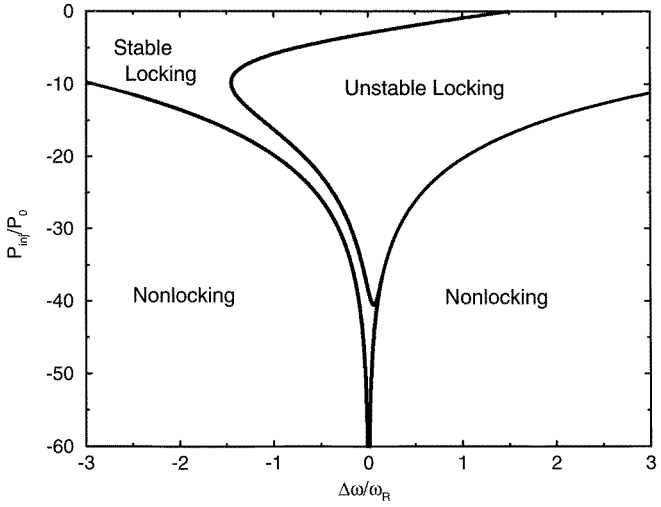

Figure 1. Locking regime and stability boundaries in $(P_{\mathrm{inj}}, \Delta\omega)$-space for an optically injected single-mode semiconductor laser. The relaxation-oscillation frequency of the free-running laser is $\omega_{\mathrm{R}}/2\pi = 5$ GHz. The parameters are given in table 1.

curves, almost symmetrically placed with respect to zero detuning, indicate the boundary of the locking regime given by equation (13), i.e. the region where locked solutions exist. The (asymmetric) inner curve is the stability boundary, given by equation (18). The asymmetry is caused by the linewidth enhancement factor α, which introduces a preference for negative detuning at higher photon densities.

4. Numerical results

Having studied the simple case of single-mode operation without taking into account spatial effects, we now return to the complete model presented in section 2. Equations (1)–(3) are solved numerically using a finite-difference method with spatial and temporal resolutions of 0.1 μm and 0.1 ps, respectively. An index-guided VCSEL with cylindrical geometry (index guiding over a 4 μm radius) is considered. The active region consists of three 8 nm quantum wells. Relevant device parameters are listed in table 1. Single-mode operation can be realized by using a disc contact of 2 μm radius such that the current is injected only over a small central part of the VCSEL top area. The LP_{01} mode is then preferentially excited. For two-mode operation, different transverse modes can be excited by two different contact geometries. A 4 μm radius disc contact excites the LP_{01} and LP_{11} modes and a ring contact of inner and outer radii of 1.8 and 2.8 μm excites the LP_{11} and LP_{21} modes. These two cases will be referred to as the disc- and ring-contact geometries, respectively, in the following sections. Since the LP_{01} and LP_{11} modes overlap slightly (weak-coupling case), whereas the LP_{11} and LP_{21} modes overlap significantly (strong-coupling case), we can assess the role of spatial hole burning and intermodal coupling on injection characteristics by comparing the results for disc- and ring-contact geometries. For two-mode operation, the two transverse modes are assumed to be orthogonally polarized, as is often observed experimentally [6]. The bias current is fixed at twice the threshold current throughout this study.

Table 1. Device parameters used in simulations.

Laser cavity length L_{eff}	2 μm
Solitary-laser round-trip time τ_{L}	0.045 ps
Active-region thickness (three QWs)	3×8 nm
Radius of device	10 μm
Radius of index-guiding region	4 μm
Diffusion constant D	30 cm^2 s^{-1}
Nonradiative recombination time τ_{e}	5 ns
Bimolecular recombination coefficient B	1×10^{-10} cm^3 s^{-1}
Refractive indices n_1, n_2	3.4, 3.5
Wavelength λ	0.875 μm
Gain cross section a_0	2.0×10^{-16} cm^2
Group velocity v_{g}	8.8×10^9 cm s^{-1}
Carrier density at transparency N_{T}	2.2×10^{18} cm^{-3}
Linewidth enhancement factor α	3
Mirror reflectivities R_1, R_2	0.995
Internal loss α_{int}	20 cm^{-1}
Longitudinal confinement factor Γ_l	0.012
Bias	$2 \times$ threshold
Injection parameter κ	1.1×10^{11} s^{-1}

4.1. Stable locking region

We first determine the stable locking region as a function of the injected power P_{inj} and frequency detuning $\Delta\nu = \Delta\omega/2\pi$ by numerically integrating equations (1)–(3). Stable locking occurs when the operating frequency of the VCSEL is locked to that of the injected signal and the output power becomes constant. In computer simulations, the output power exhibits some fluctuations because of the inherent numerical noise and we consider stable locking to occur when the time-averaged power fluctuations are smaller than 1% of the average power. Since we are interested in the possibility of turning a two-mode VCSEL into single-mode VCSEL, we choose the injected field to be linearly polarized in such a way that it couples only into one of the two modes. The optically injected mode is chosen to be the fundamental LP_{01} mode for the disc-contact case and the LP_{11} mode for the ring-contact case. By comparing the results obtained from numerical simulations and analytical solutions (discussed in the previous section), the effects of spatial hole burning and intermodal coupling can be analysed.

Figure 2 presents the results for the three cases of (i) single-mode operation, (ii) two-mode operation with two weakly coupled modes (disc contact) and (iii) two strongly coupled modes (ring contact). The full circles show the region of injection locking determined numerically and full curves show the locking boundaries obtained from the analytical solution of the spatially independent single-mode equations discussed in section 3. The injected powers P_{inj} are given in decibels (dB) relative to the free-running power P_0 of the optically injected mode. Within the range of parameters investigated, it is found that when the optically injected mode is locked to the injected signal, the other mode also shows CW operation due to intermodal coupling introduced by spatial hole burning. Numerical and analytical results show good quantitative agreement for both single-mode operation

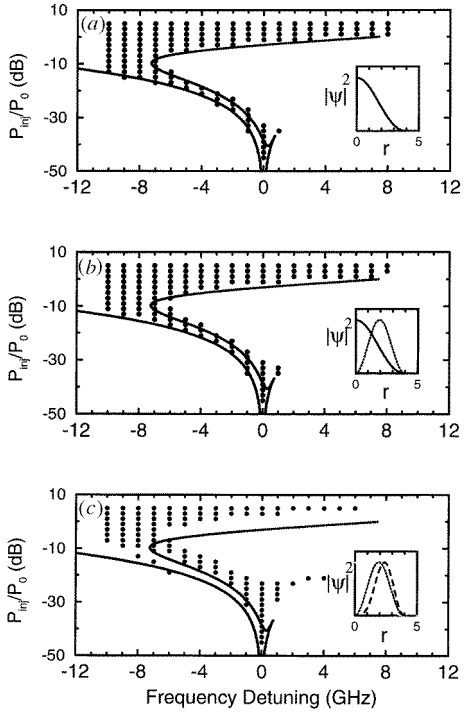

Figure 2. Stable-locking regions under injection conditions. Full circles represent the locking regions obtained numerically and full curves show, for comparison, the stability boundaries of figure 1. (*a*) Single-mode operation; two-mode operation with a (*b*) disc-contact and (*c*) ring-contact geometry. The insets show the radial-intensity profiles of the modes in each case, with full, dotted and broken curves representing the LP_{01}, LP_{11} and LP_{21} modes, respectively.

(figure 2(*a*)) and two-mode operation with the disc-contact geometry (figure 2(*b*)). The agreement for the single-mode case suggests that carrier diffusion and spatial hole burning have negligible effects on the injection-locking behaviour in single-mode VCSELs. The agreement for two-mode operation with the disc contact is surprising at first sight, but can be understood by noting that the spatial overlap between the LP_{01} and LP_{11} modes is relatively small (see the inset) and hence the intermodal coupling induced by spatial hole burning is relatively weak. In contrast, for the case of a ring-contact geometry, figure 2(*c*) shows that the locking region is lifted to higher injected powers. This difference can be understood in view of the strong coupling between the LP_{11} and LP_{21} modes induced by spatial hole burning (see the inset). Strong coupling is also responsible for extending the locking regime to the positive-frequency side at relatively low injection powers (<-20 dB).

To answer the question of whether injection locking can turn a two-mode VCSEL into a single-mode device, the mode powers are calculated for different values of injection power and frequency detuning while staying inside the locking region. For the weak-coupling case (disc contact), it is found that as the injected power is increased, the power increase in the optically injected LP_{01} mode is accompanied by a simultaneous power reduction of the LP_{11} mode, eventually leading to its complete suppression. For the case of strong intermodal coupling (ring contact), the transition from two- to single-mode operation is more abrupt, and occurs right at the lower boundary of the locking region. In both cases, calculations show that under relatively strong injection (>-10 dB), the power carried by the single injection-locked mode is larger than the total power carried by the two modes under free-running conditions plus the additional power supplied by injection. This increase in power is attributed to the decrease in power of the suppressed mode, since the carriers that were used by that mode are available for the dominant mode. Furthermore, the additional increase in single-mode power suggests that in the injection-locked state, the pump is used more efficiently. The main point to note is that, although only one mode is directly coupled to the injected field, the power in the other mode is also significantly affected due to intermodal coupling through the carrier density.

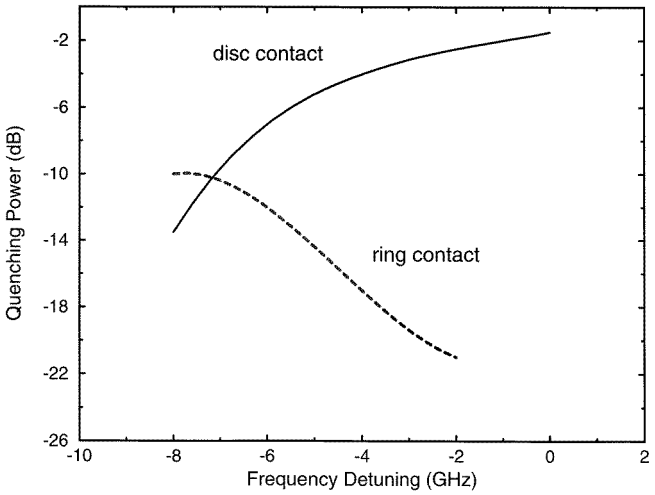

Figure 3. Change in quenching power with frequency detuning inside the stable locking region for the disc- and ring-contact geometries, respectively.

Figure 3 shows the dependence of the quenching power (beyond which one of the two modes is turned off) on frequency detuning. The exact value at which single-mode operation occurs is dependent on the frequency detuning mainly because of the change in the location of the boundary of the locking region with detuning. For the weak-coupling case (disc contact), relatively high quenching powers (>-10 dB) are required and quenching occurs only in the upper stretch of the locking region (figure 2(*b*)). As the frequency detuning is changed from -8 to 0 GHz, the quenching power increases due to the change in location of the upper boundary. In contrast, for the strong-coupling case (ring contact), much lower quenching powers (<-10 dB) are required (figure 3). Therefore, quenching can occur in both the lower and the upper parts of the locking region (figure 2(*c*)). As the injection-laser frequency approaches the frequency of the free-running mode, the quenching power decreases due to the change in location of the lower boundary. The quantitative difference between the magnitudes of the quenching power for two-mode operation with different contact geometries can be explained intuitively. Since the spatial distributions of LP_{11} and LP_{21} modes overlap much more significantly, spatial hole-burning effects are stronger, leading to stronger mode competition. Therefore, a relatively small increase in the power of the optically injected mode is adequate to turn off the other mode completely. However, for $|\Delta\nu| < 1$ GHz, quenching is no longer possible in the lower locking region (<-20 dB) and the quenching power increases significantly (>2 dB) since quenching has to occur in the upper region of figure 2(*c*).

The above analysis can be extended to the multi-mode case and a similar behaviour is expected. In essence, injection increases the power in the optically injected mode, which simultaneously suppresses the power in the other modes due to mode competition induced by spatial hole burning. The amount of suppression depends critically on the strength of spatial hole burning, the injected power and the frequency detuning.

4.2. Nonlocking region

Besides considering the practical importance of injection locking, it is also interesting to investigate the dynamics outside the locking region. We first study the dynamics inside the nonlocking region where no locked solution exists (figure 1). The injection power is chosen to be -27 dB and the temporal traces are obtained for different frequency detunings. At a relatively large detuning ($|\Delta\nu| > 7$ GHz), oscillations are close to being purely sinusoidal. For the case of two-mode operation, the two modes oscillate in phase sinusoidally. Figures 4 and 5 show the temporal traces at an injected power of -27 dB and frequency detunings of -5 and -3 GHz, respectively. Results for single- and two-mode operation with a disc and a ring contact are presented in figures (*a*)–(*c*), respectively. In all three cases (*a*)–(*c*), as the magnitude of the frequency detuning is decreased, generation of new frequency components through wave-mixing processes become more efficient, resulting in harmonic distortions. Moreover, the oscillation amplitude is enhanced when the frequency detuning approaches the relaxation-oscillation frequency (5 GHz under free-running conditions). However, for two-mode operations, the behaviours of individual modes are quite different. As the frequency detuning is changed from -5 to -3 GHz, harmonic distortions are accompanied by an increasing phase shift between the two modes because of more efficient wave mixing and stronger mode competition (figures 4(*b*), (*c*), 5(*b*), (*c*)). For the strong-coupling case (ring contact), mode competition is so intense that the power oscillations in the two modes are almost anti-correlated (figure 5(*c*)). Further, the peak-to-peak power variations as well as the amount of harmonic distortions are small compared with the disc-contact case. Evidently, strong spatial hole burning between the two highly overlapping modes results in significant

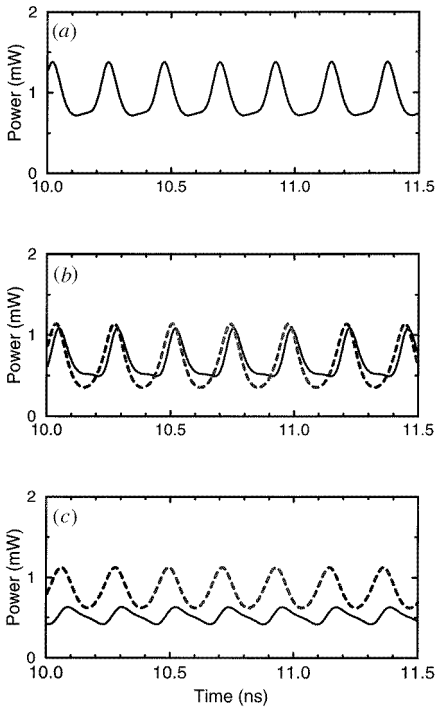

Figure 4. VCSEL dynamics in the nonlocking region. Temporal traces in a 1.5 ns temporal window at an injected power of −27 dB and a frequency detuning of −5 GHz. (*a*) Single-mode operation; (*b*) two-mode operation with a disc contact; (*c*) two-mode operation with a ring contact.

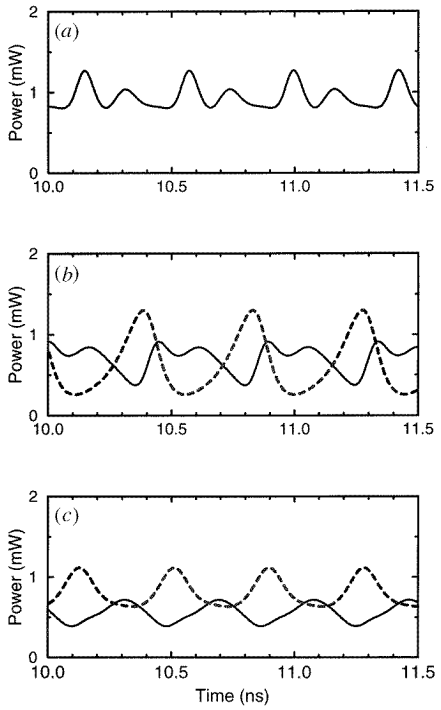

Figure 5. Operation conditions are the same as those of figure 4 except for a −3 GHz frequency detuning.

intermodal coupling so that the effective strength of the injected field seen by the VCSEL is reduced, resulting in reduced harmonic distortions.

4.3. Unstable locking region

Since qualitatively different dynamical behaviours are possible inside the nonlocking and unstable locking regions [2], we also studied the dynamics inside the unstable locking region (figure 1). To investigate the change in dynamics as one approaches the boundary between the unstable locking region and the nonlocking region (figure 1), temporal traces are computed for injection powers of −5, −10, −15 and −20 dB at a fixed frequency detuning of 5 GHz. For the single-mode case, it is found that the device exhibits period-one sinusoidal oscillations well inside the unstable locking region ($P_{\mathrm{inj}}/P_0 = -5$ dB). However, as one approaches the boundary between the unstable locking and nonlocking regions, period-four oscillations ($P_{\mathrm{inj}}/P_0 = -10$ dB) and quasi-periodic behaviours ($P_{\mathrm{inj}}/P_0 = -15$ dB) are observed. When one crosses the boundary, the quasi-periodic behaviour disappears and period-one and sinusoidal oscillations are observed ($P_{\mathrm{inj}}/P_0 = -20$ dB). Qualitatively similar results are obtained for two-mode operations. However, for the strong-coupling case (ring contact), chaos occurs at a higher injection power of ~ -10 dB. Figure 6 illustrates one set of the temporal traces inside the unstable locking region at a frequency detuning

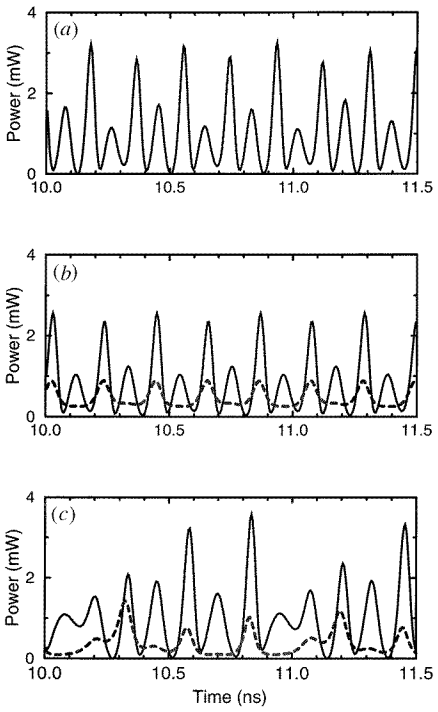

Figure 6. VCSEL dynamics in the unstable locking region. Temporal traces in a 1.5 ns temporal window at an injected power of −10 dB and a frequency detuning of 5 GHz. (*a*) Single-mode operation; (*b*) two-mode operation with a disc contact; (*c*) two-mode operation with a ring contact.

of 5 GHz and an injected power of −10 dB. The device exhibits period-four oscillations under single-mode operation (figure 6(*a*)) and the weak-coupling case (figure 6(*b*)), whereas quasi-periodic behaviour is observed for the strong-coupling case (figure 6(*c*)). These results again suggest that strong intermodal coupling makes the VCSEL less sensitive to external injection.

5. Conclusions

In conclusion, we have studied the static and dynamic characteristics of an optically injected VCSEL over a wide range of frequency detunings and injection powers. Both single- and two-mode operation are studied and compared and the role of spatial hole burning is assessed. Operation characteristics are found to be affected considerably by the strength of intermodal coupling introduced by spatial hole burning. Our results show that strong intermodal coupling reduces the sensitivity of VCSELs to external injection, in terms of both static (locking) and dynamic (nonlocking) behaviours. Specifically, it is found that strong intermodal coupling shifts the locking region up to higher injection powers. Inside the locking region, power enhancement of one mode due to injection effects results in simultaneous power reduction of the other mode. In particular, one mode can be completely suppressed depending on the strength of spatial hole burning and the injected power. Much lower quenching powers (<-10 dB) are required for the strong-coupling case due to strong mode competition induced by spatial hole burning.

Outside the locking region, the results show that the dynamics of different modes are correlated through intermodal coupling. A phase shift arises between different modes, the magnitude of which is dependent on the injected power and the strength of mode competition. Qualitatively different dynamics are observed inside the nonlocking region

and unstable locking region. Inside the unstable locking region, chaos is observed at higher injection powers for the strong-coupling case compared with the weak-coupling case. Although we have focused on the two-mode case, the qualitative nature of the results is expected to remain unaffected under multi-mode operation.

Acknowledgment

This work is partially supported by the US Army Research office.

References

[1] Lang R 1982 Injection locking properties of a semiconductor laser *IEEE J. Quantum Electron.* **QE-18** 976–83
[2] van Tartwijk G H M, Muijres G, Lenstra D, van Exter M P and Woerdman J P 1993 Semiconductor laser beyond the locking range of optical injection *Electron. Lett.* **29** 137–8
[3] Simpson T B, Liu J M, Gavrielides A, Kovanis V and Alsing P M 1995 Period-doubling cascades and chaos in semiconductor lasers subject to optical injection *Phys. Rev.* A **51** 4181–5
[4] Mori Y, Shibata J and Kajiwara T 1989 Optical polarization bistability in TM wave injected semiconductor lasers *IEEE J. Quantum Electron.* **QE-25** 265–72
[5] Chang-Hasnain C J 1995 *Semiconductor Lasers: Past, Present and Future* ed G P Agrawal (New York: AIP Press) ch 5
[6] Chang-Hasnain C J, Harbison J P, Hasnain G, Von Lehmen A C, Florez L T and Stoffel N G 1991 Dynamic, polarization and transverse mode characteristics of VCSELs *IEEE J. Quantum Electron.* **QE-27** 1402–8
[7] Li H, Lucas T L, McInerney J G, Wright M W and Morgan R A 1996 Injection locking dynamics of vertical cavity semiconductor lasers under conventional and phase conjugate injection *IEEE J. Quantum Electron.* **QE-32** 227–35
[8] Pan Z G, Jiang S and Dagenais M 1993 Optical injection induced polarization bistability in vertical-cavity surface-emitting lasers *Appl. Phys. Lett.* **63** 2999–3001
[9] Valle A, Sarma J and Shore K A 1995 Spatial hole-burning effects on the dynamics of vertical-cavity surface-emitting laser diodes *IEEE J. Quantum Electron.* **QE-31** 1423–31
[10] Morgan R A, Guth G D, Focht M W, Asom M T, Kojima K, Rogers E L and Callis S E 1993 Transverse mode control of vertical-cavity top-surface-emitting lasers *IEEE Photon. Technol. Lett.* **4** 374–7
[11] Wilson G C, Kuchta D M, Walker J D and Smith J S 1994 Spatial hole-burning and self-focusing in vertical-cavity surface-emitting laser diodes *Appl. Phys. Lett.* **64** 542–4
[12] van Tartwijk G H M and Lenstra D 1995 Semiconductor lasers with optical injection and feedback *Quantum Semiclass. Opt.* **7** 87–143
[13] Mukaihara T, Koyama F and Iga K 1992 Stress effect for polarization control of surface emitting lasers *Electron. Lett.* **28** 555–6
[14] Sun D, Towe E, Ostdiek P H, Grantham J W and Vansuch G J 1995 Polarization control of vertical-cavity surface-emitting lasers through use of an anisotropic gain distribution in (110)-oriented strained quantum-well structures *IEEE J. Sel. Topics Quantum Electron.* **1** 674–80
[15] Choquette K D, Schneider R P, Lear K L and Leibenguth R E 1995 Gain-dependent polarization properties of vertical-cavity lasers *J. Sel. Topics Quantum Electron.* **1** 661–6
[16] San Miguel M, Feng Q and Moloney J V 1995 Light polarization dynamics in surface emitting semiconductor lasers *Phys. Rev.* A **52** 1728–39
[17] Pippard A B 1985 *Response and Stability: an Introduction to the Physical Theory* (Cambridge: Cambridge University Press) pp 25–30